Fluid Dynamics &
Materials Processing

Tech Science Press

http://doi.org/10.32604/fdmp.2026.079253

ARTICLE

A Coupled Model for Multi-Component Gas Wellbore Thermo-Pressure Behavior

Xiang Li[1,2], Jie Zhang[1,2,*], Yuxin Cheng[1,2], Jiaohao Xie[1,2] and Zhaoqi Xiong[1,2]

[1]State Key Laboratory of Oil and Gas Reservoir Geology and Exploitation, Southwest Petroleum University, Chengdu, China
[2]Petroleum Engineering School, Southwest Petroleum University, Chengdu, China
*Corresponding Author: Jie Zhang. Email: swpivip@163.com

Received: 18 January 2026; Accepted: 28 April 2026; Published: 27 May 2026

ABSTRACT: Current prediction methods for wellbore temperature and pressure in gas storage injection–production wells are commonly based on the simplifying assumption of pure methane, thereby neglecting the multi-component nature of real natural gas and limiting predictive accuracy. To overcome this shortcoming, this study develops a comprehensive model for the coupled temperature and pressure fields in wellbores transporting multi-component natural gas mixtures. The proposed framework explicitly accounts for compositional effects by integrating key thermophysical properties, including density, viscosity, compressibility factor, and Joule–Thomson coefficient, into the governing flow equations, thereby enhancing the fidelity of the ensuing injection and production process simulations. The resulting system of equations is solved numerically using a fourth-order Runge–Kutta scheme. Validation against field data from the Xiangguosi Gas Storage facility demonstrates strong agreement, with prediction errors for both temperature and pressure remaining within 3%. Furthermore, sensitivity analyses are presented for representative field conditions, thereby elucidating the roles of principal controlling factors in shaping the wellbore thermo-pressure behavior, and offering valuable theoretical and practical insights for operational optimization and safety management.

KEYWORDS: Mixed gas; gas storage; dynamic physical properties parameters; temperature prediction; pressure field

1 Introduction

As global energy systems transition toward clean and low-carbon sources, natural gas serves as a pivotal bridge linking conventional energy and renewable energy sources. Its supply security and peak shaving and supply assurance capabilities have increasingly become a core strategic priority underpinning national economic development [1,2]. As the most critical and high-efficiency peak-shaving infrastructure across the natural gas value chain, gas storage mitigates the inherent spatial and temporal mismatch in natural gas demand through its cyclic injection and production regime of summer injection and winter production, while fulfilling an irreplaceable role in addressing extreme weather events and emergency supply disruptions [3–5].

Heat transfer and flow within wellbores constitute a strongly coupled process. A fundamental framework for the analysis of heat transfer in wellbores has been established in previous studies. A classical model was first proposed by Ramey [6], and Satter [7] then modeled the dynamics as a steady-state process and introduced a dimensionless time function to describe formation heat transfer as an unsteady state. These works have provided a strong foundation for subsequent research. The effectiveness of the models was subsequently

verified by Holst [8], and their efficacy has been widely recognized in the field. Later, Orkiszewski [9] analyzed field data from 148 wells and developed a pressure calculation model in which different pressure patterns are selected according to the flow regime of the fluid. Farouq [10] developed a similar discretized model using a finite-difference method. However, conventional models typically fail to fully account for the effects of coupling between temperature and pressure because they calculate the two parameters separately.

Recently, models that couple temperature and pressure have been developed to enhance prediction accuracy based on more advanced techniques for numerical computation [11]. Sang et al. [12] developed such a model for steam injection based on the conservation of energy, mass, and momentum. AI-Adwani et al. [13] found that the injection of carbon dioxide is associated with overall heat transfer and proposed an improved model based on the Span [14] state equation. Along similar lines, Liu et al. [15] discovered that temperature and pressure exhibit mutual coupling effects during production in gas wells. Consequently, they developed a formulation that couples thermal and hydraulic effects for single-phase flow and applied it to analyze the influence of production rates on temperature and pressure at wellbore sites. To investigate the impact of key factors on the distribution of temperature and pressure inside a wellbore, Zuo et al. [16] solved a coupled model using a piecewise iterative method and verified that the model exhibited high accuracy. In a more recent study, Hong et al. [17] proposed a high-temperature and high-pressure (HTHP) coupled model, and their results further demonstrate the importance of considering interactions between thermal and fluid dynamics in underground gas storage wells.

Despite significant progress in existing research on temperature-pressure coupling and numerical solutions, two major limitations remain. First, natural gas is conventionally simplified as a single gas with constant physical parameters, which neglects variations in the actual composition of mixed gases and their strongly nonlinear dynamic characteristics. Second, the mechanisms of the influence of the relevant parameters have not been systematically quantified in the literature. Existing analyses are often limited to qualitative or localized insights and generally fail to reveal how key variables affect the distribution of temperature and pressure throughout the wellbore in a holistic manner. In this study, a transient fully coupled prediction model for wellbore operations that integrates dynamic physical properties of mixed gases is proposed to resolve these problems. The proposed approach obviates the need for the assumption that natural gas contains only methane by establishing a dynamic model to calculate the physical properties of real natural gas with multiple different components. To that end, the temperature-pressure coupling equations are solved in real time via iterative calculations. The results reveal patterns of dynamic variation of mixed gases along the wellbore. Consequently, the impact of key parameters on the temperature-pressure field is systematically quantified. These include the temperature and pressure during injection and production, along with the quantity of gas injected and the composition of the gas inside the wellbore. The results of a numerical validation based on field data demonstrate the high accuracy and strong practical applicability of the model. Thus, the proposed approach establishes a sound theoretical basis to optimize injection-production plans for gas storage facilities and to manage wellbore integrity.

2 Calculation of the Physical Properties of Gas Mixtures

Accurate dynamic calculation of natural gas physical properties is a critical factor in ensuring the accuracy of transient wellbore modeling predictions. Natural gas is not composed solely of methane; rather, it also contains other components, including carbon dioxide and nitrogen. The concentration of each component affects the physical properties of the natural gas and thereby alters flow and heat transfer behavior within a wellbore. Therefore, this section describes the proposed method for calculating the physical properties of natural gas containing trace gases in wells for storage reservoirs. The proposed approach thus avoids errors

that are introduced in conventional models due to their assumption of constant physical properties and a pure methane composition of natural gas.

2.1 Calculation of Critical Parameters for Gas Mixtures

The following mixing rules are applied as a basis for calculating the physical properties of a given gas mixture by obtaining its virtual critical parameters [18].

$$T_{cm} = \sum_{i=1}^{n} \sum_{j=1}^{n} \left[y_i y_j (T_{ci} T_{cj})^{0.5} \left(1 - k_{ij}\right) \right] \tag{1}$$

$$P_{cm} = \frac{\sum_{i=1}^{n} \sum_{j=1}^{n} \left[y_i y_j (T_{ci} T_{cj})^{0.5} \left(1 - k_{ij}\right) \right]}{T_{cm} \sum_{i=1}^{n} \frac{y_i}{T_{ci}}} \tag{2}$$

where y_i and y_j are the molar fractions of components i and j (dimensionless), T_{ci} and T_{cj} denote their critical temperatures and critical pressures, respectively (K), and k_{ij} is a dimensionless binary interaction coefficient.

The average molar mass is calculated using the linear addition rule:

$$M_m = \sum_{i=1}^{n} (y_i M_i) \tag{3}$$

where M_m is the molar mass of the gas mixture (kg/mol).

2.2 Calculation of the Compression Factor for Mixed Natural Gas

In the natural gas industry, the compression factor [19] is often referred to as the deviation factor. This parameter describes the physical differences between real and ideal gases, and its numerical value is defined as the ratio of the actual volume of a gas to the volume it would occupy as an ideal gas. Thus, the compression factor is a key element in measuring the compressibility of gases. Once the pseudocritical parameters of a given mixture are obtained, its relative temperature and pressure are calculated as given below.

$$T_r = \frac{T}{T_{cm}} \tag{4}$$

$$P_r = \frac{P}{P_{cm}} \tag{5}$$

where T_r is relative temperature (K) and P_r is relative pressure (MPa).

The compression factor is calculated using the cubic Peng-Robinson (PR) equation of state, which is written as:

$$P = \frac{RT}{V_m - b_m} - \frac{a_m(T)}{V_m(V_m + b_m) + b_m(V_m - b_m)} \tag{6}$$

Its parameters are defined as follows:

$$a_m(T) = \sum \sum y_j y_i a_{ij}(T) \tag{7}$$

$$b_m = \sum y_i b_i \tag{8}$$

$$a_{ij}(T) = \left(1 - k_{ij}\right)\sqrt{a_i(T)a_j(T)} \tag{9}$$

$$Z_m = \frac{PV}{RT} \tag{10}$$

where Z_m is the compression factor of the mixed gas (dimensionless).

The compression factor equation can be derived from the PR equation:

$$Z_m{}^3 - (1 - B_m)Z_m{}^2 + \left(A_m - 3B_m{}^2 - 2B_m\right)Z_m - \left(A_mB_m - B_m{}^2 - B_m{}^3\right) = 0 \tag{11}$$

where:

$$A_m = \frac{a_m(T)P}{(RT)^2} \tag{12}$$

$$B_m = \frac{b_mP}{RT} \tag{13}$$

In the proposed numerical solution process, the compression factor is updated in real time at each iteration within every depth step by solving the PR equation of state evaluated at the current local pressure and temperature. This enables precise calculation of gas density and molar volume and thus provides critical inputs for the momentum and energy equations.

2.3 Density and Viscosity of Mixed Natural Gas

The density [20] of a mixed gas can be directly determined using the ideal gas equation using the calculated mixed compression factor as given below.

$$\rho_m = \frac{PM_m}{Z_mRT} \tag{14}$$

where ρ_m is the density of the gas mixture (kg/m^3).

The viscosity [21] of natural gas is a physical parameter that measures its internal frictional resistance or ability to resist shear deformation. It is inversely proportional to the flowability of the fluid. This parameter is significantly influenced by the operating conditions; at low pressures, viscosity is insensitive to changes in pressure and primarily increases with rising temperature. In contrast, it rises with increasing pressure or gas molecular weight at high pressures but decreases with rising temperature. Viscosity is calculated as given below [22].

$$\mu_g = 10^{-4}Kexp\left(X\rho_g^Y\right) \tag{15}$$

where:

$$K = \frac{\left(22.650 + 0.0388M_g\right)T^{1.5}}{\left(209.2 + 19.26M_g + 1.8T\right)} \tag{16}$$

$$X = 3.448 + 548 + 0.01M_g \tag{17}$$

$$Y = 2.447 - 0.224X \tag{18}$$

$$\rho_g = 3.4844\frac{\gamma_g p}{ZT} = 0.12037\frac{pM_g}{ZT} \tag{19}$$

where μ_g and ρ_g are, respectively, the density (kg/m^3) and viscosity (mPa·s) of the natural gas, γ_g is the relative density (dimensionless), p and T are the wellbore pressure (MPa) and temperature (K), respectively, and M_g is the average molecular mass of the mixture (kg/mol).

Fig. 1 illustrates the variation in the viscosity of natural gas.

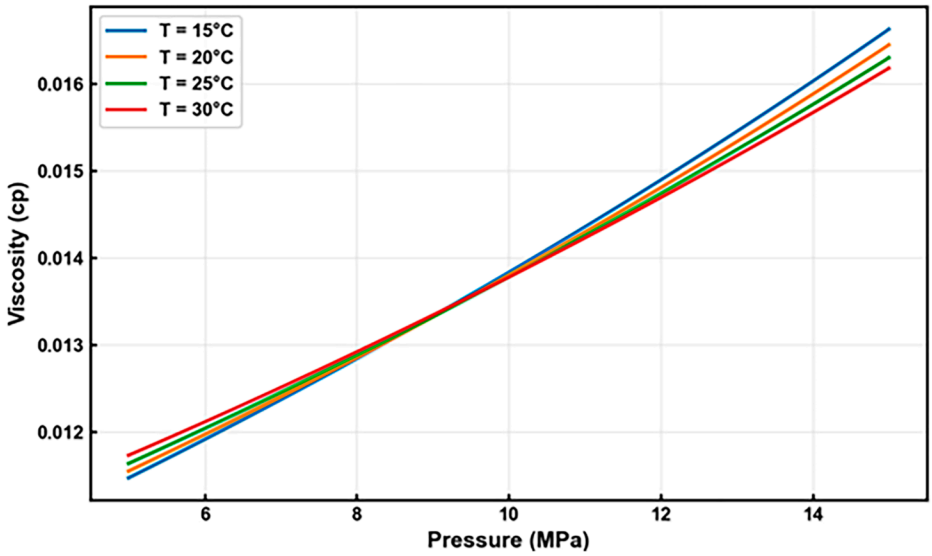

Figure 1: Natural gas viscosity as a function of temperature and pressure.

Fig. 1 shows that, at a constant temperature, the viscosity of natural gas increases with increasing pressure. The curved surface shows a distinct upward trend along the pressure axis, which indicates that, in a high-pressure environment, the distance between gas molecules decreases and the interaction intensifies, which results in an increase in viscosity. Under low pressure, the viscosity of natural gas increases with increasing temperature. In contrast, under high pressure, the distance between gas molecules is reduced significantly, and the viscosity of natural gas gradually decreases as temperature rises.

2.4 Joule-Thomson Coefficient

The Joule–Thomson (JT) coefficient [23] indicates the change in temperature per unit pressure drop under isenthalpic conditions.

$$\mu_J = \left(\frac{\partial T}{\partial P}\right)_p \tag{20}$$

where μ_J is the JT coefficient (K/MPa).

This coefficient characterizes variations in the temperature of an actual gas during the flow process and is a key parameter in fields such as natural gas processing and refrigeration engineering [24].

It is typically obtained from the definition of the JT coefficient and the principles of thermodynamics as follows:

$$\mu_J = \frac{1}{C_p} T\left[\left(\frac{\partial T}{\partial P}\right)_p - v\right] \tag{21}$$

The PR equation of state is adopted in the proposed approach to describe actual gas behavior. Substituting pv = ZRT into the above equation, we obtain:

$$\mu_J = \frac{1}{C_p p}\left(\frac{\frac{RT}{V-b} - \frac{1}{V(V+b)+b(V-b)} T\frac{\mathrm{d}a}{\mathrm{d}T}}{\frac{RT}{(V-b)^2} - \frac{2a(2+b)}{[V(V+b)+b(V-b)]^2}} - V\right) \tag{22}$$

As shown in Fig. 2, the JT coefficient of methane demonstrates a clear dependence on both temperature and pressure. Under constant pressure conditions, the coefficient decreases with increasing temperature. Similarly, at a constant temperature, it decreases as pressure increases, which indicates an inverse correlation with both variables.

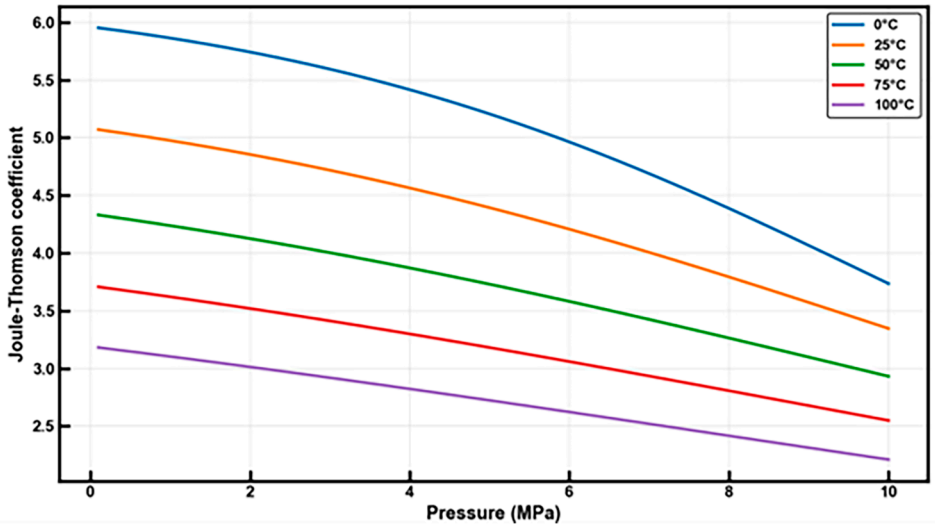

Figure 2: Variation of Joule-Thomson coefficients with temperature and pressure.

3 Mathematical Model

3.1 Assumed Conditions

Flow and thermal behavior within the wellbore is a highly intricate process [25], rendering it extremely challenging to investigate with full accuracy. Thus, the following assumptions are adopted to simplify the analysis while maintaining engineering relevance.

Assumption 1: *The rate of radial heat transfer is significantly higher than that of axial transfer. Therefore, longitudinal conduction of the gas in the direction of the fluid flow can be neglected. To model the heat transfer as a simplified one-dimensional steady-state process, the inner and outer faces of the tubing and casing are considered to remain at uniform temperatures or under uniform heat exchange conditions.*

Assumption 2: *Heat transfer between formations is modeled as an unsteady-state process, and the formations are homogeneous with no internal heat sources.*

Assumption 3: *The gas within the wellbore primarily flows axially and can be simplified as one-dimensional compressible fluid flow along the direction of the depth of the well.*

Assumption 4: *The tubing, casing, and cement ring form concentric cylindrical structures.*

These assumptions are commonly adopted in models of heat transfer in wellbores to facilitate practical engineering calculations. The present model is primarily applicable to conventional underground gas storage injection-production wells.

Fig. 3 presents a schematic of a wellbore control unit, along with the structure of a wellbore in an injection-production well. A cylindrical control body of length dz is taken from the wellbore. Moreover, a cylindrical coordinate system is established with the direction of the axis of the wellbore set as the positive z-axis to align with the direction of the gas flow. A systematic set of governing equations describing gas flow and heat transfer is thus established by analyzing this control body.

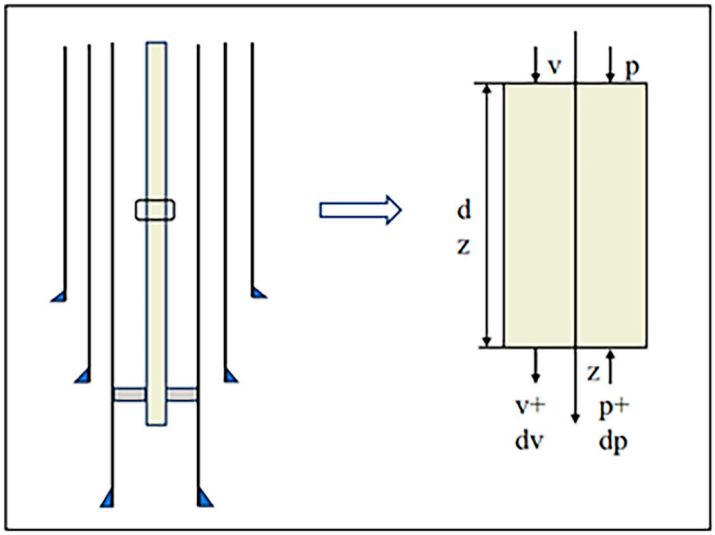

Figure 3: Diagram of the unit control body.

3.2 Temperature and Pressure Distributions

3.2.1 Energy Conservation Equation

In fluid micro-element analysis, the law of conservation of energy must be satisfied for an isolated control body, the internal energy of which varies at a rate matching the net rate of energy inflow. The energy loss caused by factors such as friction and heat transfer must also be taken into consideration.

$$h(z) + \frac{1}{2}v^2(z) + gz = h(z + \mathrm{d}z) + \frac{1}{2}v^2(z + \mathrm{d}z) + g(z + \mathrm{d}z) + q \tag{23}$$

where m is the mass of the fluid (kg), g is the gravitational acceleration near Earth's surface (9.8 m/s^2), v is the fluid velocity (m/s), q is the heat per unit mass (J/kg), and z is the length of the wellbore (m).

Furthermore, the above equation can be rewritten as a differential equation as follows.

$$-\mathrm{d}q = \mathrm{d}h + v\mathrm{d}v + g\mathrm{d}z \tag{24}$$

where h is the specific enthalpy (J/kg).

The heat loss from the micro-element wellbore section is equal to the heat transferred by the fluid to the outer wall of the wellbore. This quantity can be obtained as follows:

$$\mathrm{d}q_1 = \frac{2\pi r_{ti} U(T - T_{cem})}{W}\mathrm{d}z \tag{25}$$

where r_{ti} is the inner radius of the tubing (m), U is the overall heat transfer coefficient (W/(m·K)), T is the temperature in the wellbore (K), T_{cem} is the temperature at the outer edge of the cement ring (K), and W is the mass flow rate (kg/s).

The heat transfer from the outer surface of the cement ring to the formation in the micro-element wellbore section is given as:

$$\mathrm{d}q_2 = \frac{2\pi k(T_{cem} - T_e)}{f(t_D)}\mathrm{d}z \tag{26}$$

where T_e is the formation temperature (K), k is the thermal conductivity of the formation (W/(m·K)), $f(t_d)$ is the dimensionless time function for unsteady heat transfer in the formation (dimensionless).

The dimensionless time function [26] is calculated as:

$$f(t_d) = \begin{cases} (0.4063 + 0.5\ln t_d)\left(1 + \frac{0.6}{t_d}\right), & t_d > 1.5 \\ 1.1281\sqrt{t_d}(1 - 0.3\sqrt{t_d}), & 10^{-10} \le t_d \le 1.5 \end{cases} \tag{27}$$

$$t_d = \frac{\alpha t}{r_h^2} \tag{28}$$

where α is the thermal diffusivity of the formation (m^2/s), t is the production time (s), r_h is the radius of the cement sheath (m), and t_d is the dimensionless temperature for formation heat conduction.

Thermal diffusivity of formation [27] α is given as:

$$\alpha = \frac{k_e}{(\rho c)_e} \tag{29}$$

where $(\rho c)_e$ is effective volumetric heat capacity of the formation ($J\cdot m^{-3}\cdot K^{-1}$).

According to fundamental laws of thermodynamics, calculation method of enthalpy is:

$$\mathrm{d}h = \left(\frac{\partial h}{\partial T}\right)_p \mathrm{d}T + \left(\frac{\partial h}{\partial p}\right)_T \mathrm{d}p = c_p \mathrm{d}T - \alpha_J c_p \mathrm{d}p \tag{30}$$

The temperature control equation obtained during gas injection is given as follows:

$$\frac{\mathrm{d}T}{\mathrm{d}z} = \mu_J \frac{\mathrm{d}p}{\mathrm{d}z} + \frac{v^2}{\rho C_p}\frac{\mathrm{d}\rho}{\mathrm{d}z} + \frac{g}{C_p} - \frac{B}{C_p}(T - T_e) \tag{31}$$

where:

$$B = \frac{2\pi r_{ti} U k_e}{\omega(r_{ti} U f(t_d) + k_e)} \tag{32}$$

Similarly, the temperature control equation during gas extraction can be obtained as:

$$\frac{\mathrm{dT}}{\mathrm{d}z} = \mu_J \frac{\mathrm{d}p}{\mathrm{d}z} + \frac{v^2}{\rho C_p}\frac{\mathrm{d}\rho}{\mathrm{d}z} - \frac{g}{C_p} - \frac{B}{C_p}(T - T_e) \tag{33}$$

3.2.2 Heat Transfer Model

When gas is injected from an oil pipe, it will transfer heat energy to the formation. The process of heat transfer is modeled as a series of sub-processes with multiple successive links. This process can be decomposed into four main stages, including convective heat exchange between the gas and the inner wall of tubing, radial heat conduction of the oil pipe wall, coupled convective and radiative heat transfer within the annular medium, radial heat conduction of the casing wall, and finally the process of thermal conduction in which heat energy enters the formation through the cement ring [28]. Fig. 4 shows the complete process of heat transfer between wellbore fluids and the formation.

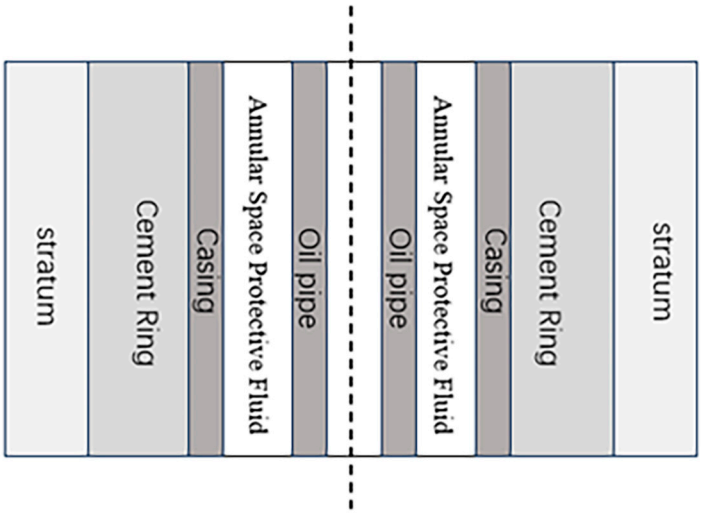

Figure 4: Heat transfer process of fluid in wellbore.

From a physical perspective, the formation is essentially infinite in extent. This characteristic dictates that the heat transfer is an unsteady-state process, with the wellbore heat flux varying dynamically across different times and locations. To simplify the calculations, this process is typically divided spatially into two parts: heat transfer occurs first from the fluid in the wellbore to the outer edge of the cement ring, followed by transfer from the edge of the cement ring to the formation, which is modeled as infinite. The former is often referred to as intra-wellbore heat transfer, while the latter is called formation heat transfer. To simplify the calculations, Satter proposed the following crucial assumption regarding this heat transfer process: heat transfer from the cement ring to the formation is considered an unsteady-state process due to geological heterogeneity, while the tubing, casing, and cement ring are considered concentric cylindrical structures to calculate the intra-wellbore heat transfer as a steady-state process. This assumption was later extensively validated by Holst and has gained widespread acceptance. However, it is vital to clarify that modeling the heat transfer within the wellbore as a steady-state process does not imply that the wellbore temperature is constant. Rather, this variation is transmitted to the wellbore because the temperature at the external boundary of the cement ring varies according to an unsteady-state process in the formation, which causes the heat flux and the temperature within the wellbore to vary accordingly. This type of wellbore

heat transfer governed by the boundary conditions of the formation is therefore more accurately described as quasi-steady-state heat transfer.

(1) The heat flow through the wall of the oil pipe is given as:

$$\frac{\partial Q}{\partial z} = \frac{2\pi k_{tub}(T_{ti}(z) - T_{to}(z))}{\ln\frac{r_{to}}{r_{ti}}} \tag{34}$$

where k_{tub} is the convective heat transfer coefficient of the tubing inner wall (W/(m^2·K)).

(2) The heat flow through the casing wall is given as:

$$\frac{\partial Q}{\partial z} = \frac{2\pi k_{cas}(T_{ci}(\mathrm{z}) - T_{co}(z))}{\ln\frac{r_{co}}{r_{ci}}} \tag{35}$$

where k_{cas} is the thermal conductivity of the casing (W/(m·K)).

(3) The heat flow through the annulus is given as:

$$\frac{\partial Q}{\partial z} = 2\pi k_{cem}(T_{to}(\mathrm{z}) - T_{ci}(z))(h_c + h_r) \tag{36}$$

where h_r is the radiative heat transfer coefficient in the annulus (W/(m^2·K)), and h_c is the convective heat transfer coefficient in the annulus (W/(m^2·K)).

(4) The heat flow through the cement ring is given as:

$$\frac{\partial Q}{\partial z} = \frac{2\pi k_{cem}(T_{co}(z) - T_h(z))}{\ln\frac{r_h}{r_{co}}} \tag{37}$$

where k_{cem} is the thermal conductivity coefficient of the cement ring (W/(m·K)).

Combining the above equations yields the following:

$$U^{-1} = \frac{r_{to}}{r_{ti}k_t} + \frac{r_{to}}{k_{tub}}\ln\frac{r_{to}}{r_{ti}} + \frac{1}{h_r + h_c} + \frac{r_{to}}{k_{cas}}\ln\frac{r_{co}}{r_{ci}} + \frac{r_{to}}{k_{cem}}\ln\frac{r_h}{r_{co}} \tag{38}$$

Due to the completion configuration of natural gas storage injection–production wells, at a given well depth z, the radial heat flow may successively pass through different numbers of casing strings and cement sheath layers. Therefore, the total thermal resistance of the system from the interior of the wellbore to the surrounding formation is equal to the sum of all the individual thermal resistances connected in series.

$$U^{-1} = \frac{r_{to}}{r_{ti}k_t} + \frac{r_{to}}{k_{tub}}\ln\frac{r_{to}}{r_{ti}} + \frac{1}{h_r + h_c} + \sum_{1}^{n}\frac{r_{to}}{k_{cas}}\ln\frac{r_{co}}{r_{ci}} + \sum_{1}^{n}\frac{r_{to}}{k_{cem}}\ln\frac{r_h}{r_{co}} \tag{39}$$

Some significant differences in terms of the respective weights of the influence of each item among the thermal resistance compositions mentioned above are of note. The convective heat transfer caused by phase change in the oil pipe has an extremely high surface heat transfer coefficient, and the corresponding thermal resistance is extremely small. Tubing and casing walls made of metal materials have a relatively low thermal resistance due to their high thermal conductivity. These thermal resistances account for a very

small proportion of the total thermal resistance and are secondary factors. Therefore, they can usually be ignored in actual calculations.

3.2.3 Momentum Conservation Equation

During gas injection into the wellbore, the flow of the fluid follows the fundamental law of the conservation of momentum. For one-dimensional steady-state flow, the equation of the conservation of momentum along the direction of the depth of the wellbore describes the composition of the pressure gradient. This is the core theoretical basis for the dynamic prediction of wellbore pressure and process design.

Treating the gas-phase pipe flow as a one-dimensional steady flow, a control segment of length dz is considered in the flow direction. By Newton's second law, the resultant external force on the control volume is equal to the rate of change of its momentum. Since the flow is steady, the local acceleration term is zero, and the convective term thus suffices to represent the change in momentum.

After accounting for the effects of pressure, gravity, and friction from contact with the pipe wall the momentum control equation for the flow can be derived. As this derivation constitutes a fundamental concept, it has been discussed in detail in the context of numerous wellbore flow models. During gas injection, the wellbore pressure gradient [29] is expressed as:

$$\frac{1}{\rho}\frac{\mathrm{d}p}{\mathrm{d}z} = g - \frac{fv^2}{4r_{ii}} - v\frac{\mathrm{d}v}{\mathrm{d}z} \tag{40}$$

Similarly, during gas production, the wellbore pressure gradient can be expressed as:

$$\frac{1}{\rho}\frac{\mathrm{d}p}{\mathrm{d}z} = g + \frac{fv^2}{4r_{ii}} + v\frac{\mathrm{d}v}{\mathrm{d}z} \tag{41}$$

In the present transient model, the one-dimensional wellbore momentum equation is applied under the assumption of a quasi-steady state because pressure disturbances propagate along the wellbore much faster than the characteristic timescale of temperature variation, which allows the transient acceleration term to be neglected. Consequently, the governing equation reduces to a commonly used steady-state form that has been widely adopted in analyses of wellbore flow.

The friction coefficient f between the gas and the pipe wall is calculated as follows using Jain's empirical formula [30]:

$$\frac{1}{\sqrt{f}} = 1.14 - 2\log_{10}\left(\frac{\varepsilon}{2r_{ti}} + \frac{21.25}{Re^{0.9}}\right) \tag{42}$$

where Re is the Reynolds number of the gas flow (dimensionless), ε is the absolute roughness of the pipe wall (mm).

4 Model Solution and Verification

4.1 Initial Conditions and Boundary Conditions

Taking the gas injection process as an illustrative example, the wellhead ($z = 0$) is set as the starting point for the calculation. Its injection temperature and pressure T_0 and P_0 can be measured directly. Therefore, the boundary conditions at the wellhead are:

$$T(z = 0) = T_{in} \tag{43}$$

$$P(z = 0) = P_{in} \tag{44}$$

Assuming a linear distribution with depth, the formation temperature can be determined using the geothermal gradient as follows:

$$T_e = T_{surface} + g_e z \tag{45}$$

where g_e is the geothermal gradient (°C/m), z is the depth of the well (m), and $T_{surface}$ is surface temperature (°C).

For each depth step (from node i to $i + 1$), the initial conditions are established for the current computational segment based on wellhead temperature, pressure, and the results from the previous time step.

4.2 Model Solution

The proposed approach applies a fourth-order Runge-Kutta method combined with an iterative advancement strategy to solve coupled systems of differential equations. Its core innovation lies in seamlessly integrating the dynamic calculation module for parameters representing the physical properties established in Chapter 1 into the solution loop. Starting from the wellhead, the steps in the downward calculation of wellbore temperature and pressure are illustrated in Fig. 5.

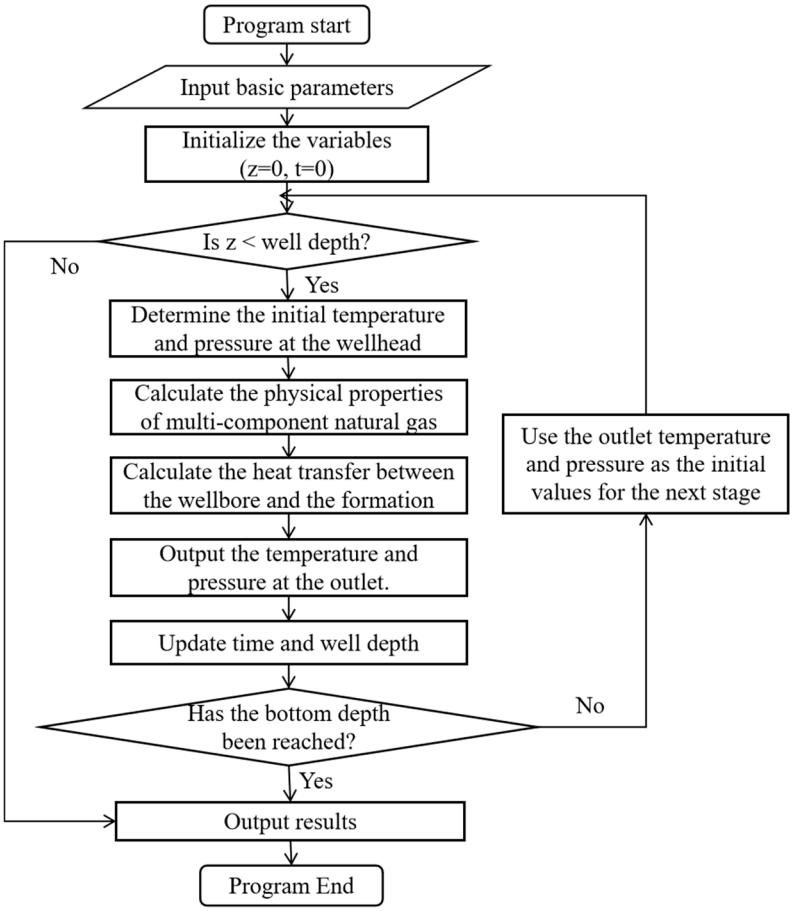

Figure 5: Flowchart of the calculation process of the model.

4.3 Model Verification

To evaluate the accuracy of the proposed wellbore heat transfer model, an experimental validation was conducted using data from a well in the Xiangguosi Gas Storage facility. The analysis examined the distribution of the temperature in the wellbore during the injection and production operations. Table 1 lists the relevant parameters for this well.

Table 1: Basic data.

Parameter Name	Value
Well depth (m)	2496.60
Cement outer diameter (mm)	320
Tubing inner diameter (mm)	99.57
Tubing outer diameter (mm)	114.3
Casing inner diameter (mm)	220.5
Casing outer diameter (mm)	273.0
Injection pressure (MPa)	24.80
Gas injection flow rate (10^4 (m^3/d))	40
Gas production flow rate (10^4 (m^3/d))	80
Bottom hole flow pressure (MPa)	28.0
Temperature of injected natural gas (°C)	35.0
Gas injection time (d)	50
Gas extraction time (d)	20

Representative natural gas components with typical reservoir characteristics were employed in the calculations. The specific components are listed in Table 2.

Table 2: Natural gas components.

Natural Gas Components	Component Content (%)
CH_4	95
CO_2	3
N_2	2

The results for the temperature and pressure distribution of the gas calculated using data from this well are shown in Fig. 6. The temperature distribution during gas production is illustrated in Fig. 7.

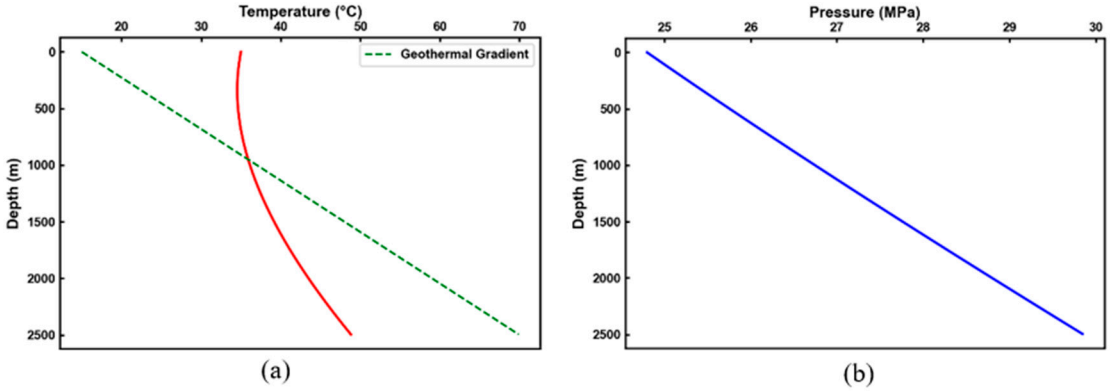

Figure 6: (**a**) Temperature and (**b**) pressure distributions along the depth of the wellbore during the injection process.

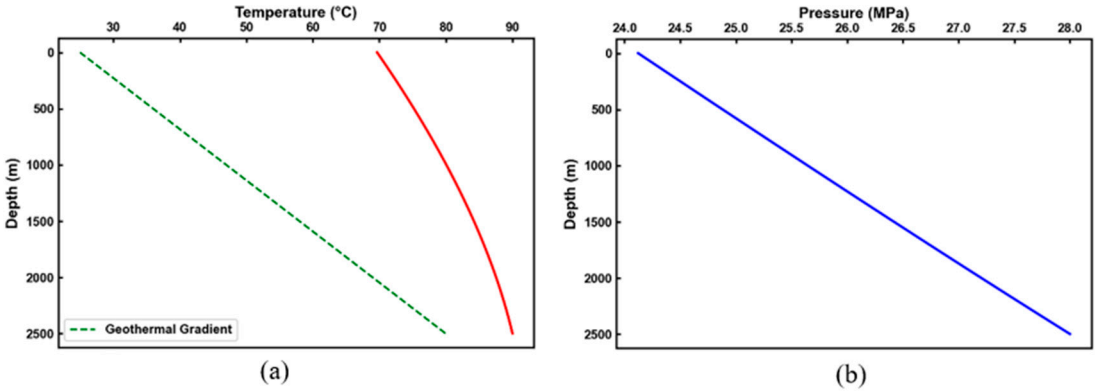

Figure 7: (**a**) Temperature and (**b**) pressure distributions along the depth of the wellbore during the production process.

Table 3 presents a comparison of the wellhead temperature and pressure predicted using a dedicated computational program developed based on the proposed mathematical model with the simulation outputs from the commercial simulation software WellCat. The prediction errors of the proposed model for both the wellhead temperature and pressure were within 3%, validating the reliability and accuracy of the proposed mathematical model and calculation method.

From the perspective of engineering applications, a prediction error within 5% is generally considered acceptable in coupled temperature-pressure simulations. The error obtained in this study was significantly lower than this engineering standard, which demonstrates the high predictive accuracy of the proposed temperature-pressure prediction model. Furthermore, the proposed model exhibited higher accuracy in temperature prediction compared with the simulation results obtained using WellCat under identical operating conditions. This reflects the advantages gained by considering the real gas equation of state, the Joule-Thomson effect, and the mechanism of heat transfer within the wellbore.

Table 3: Temperature and measured value errors.

	Measured Value	Proposed Model	WellCat
Temperature/°C	69.53	69.66	66.10
Relative error/%	-	0.18	5.19
Pressure/MPa	24.65	24.12	23.27
Relative error/%	-	2.11	5.60

5 Sensitivity Analysis

Given that the model was validated as described above, a case study of a typical X gas storage facility is presented. This is a depleted hydrocarbon reservoir-type facility reconstructed from the main block of a mature depleted gas field. It is located in the central North China Plain, with a reservoir distribution area of approximately 8.5 km^2. Because of its representative geological conditions and operational features, the site is an ideal prototype for analyzing the characteristic variations in the wellbore temperature and pressure during gas injection and production.

Numerical simulations of variations in the wellbore temperature and pressure during gas injection were carried out based on the operational parameters of the facility, and the influence of key parameters was analyzed. The core input parameters for the simulations are listed in Table 4.

Table 4: Relevant data of X gas storage facility.

Parameter name	Value
Well depth (m)	1150
Cement outer diameter (mm)	514
Tubing inner diameter (mm)	162
Tubing outer diameter (mm)	178
Casing inner diameter (mm)	257
Casing outer diameter (mm)	273
Injection pressure (MPa)	10
Gas injection flow rate (m^3/d))	4.26×10^4
Temperature of injected natural gas (°C)	20
Surface temperature (°C)	20
Geothermal gradient	0.022
Gas injection time (d)	39
Gas extraction time (d)	20
Gas production flow rate (m^3/d))	10×10^4
Formation static temperature (°C)	45.3
Bottom hole flow pressure (MPa)	11
Formation thermal diffusivity ($m^2 \cdot s^{-1}$)	1.03×10^6
Tubing thermal conductivity ($W \cdot (m \cdot K)^{-1}$)	45.35
Casing thermal conductivity ($W \cdot (m \cdot K)^{-1}$)	45.35
Cement sheath thermal conductivity ($W \cdot (m \cdot K)^{-1}$)	0.983
Formation thermal conductivity ($W \cdot (m \cdot K)^{-1}$)	2.06
Annular fluid thermal conductivity ($W \cdot (m \cdot K)^{-1}$)	0.60
Friction coefficient of the pipe wall	0.015

Data analysis was conducted using gas injection parameters for the target well from a specific period in 2022. The storage reservoir operates at pressures ranging from 5 to 12 MPa.

The influence of key injection parameters on the transient wellbore behavior was quantitatively evaluated by applying the present model to predict the wellbore temperature and pressure distributions under different injection temperatures and pressures. The simulation results allow for a direct identification of operating conditions under which the bottomhole pressure may approach or exceed the upper pressure limit. Based on these predictions, appropriate combinations of injection temperatures and pressures can be selected to ensure that the wellbore pressure remains within the safe operating range.

A sensitivity analysis was conducted to systematically quantify the impact of key parameters. Variations in some specific parameters considered in the sensitivity analysis are shown in Table 5. The selected parameter ranges reflect the operating conditions of gas injection wells, including variations in injection pressure, injection temperature, injection quantity, geothermal gradient, and gas composition. The ranges were used to analyze the potential influence of each parameter on the distribution of temperature and pressure within a given wellbore.

Table 5: Values of different parameters.

Pressure/MPa	Temperature/°C	Gas injection flow rate/10^4(m^3/d)	Geothermal gradient	Natural Gas Components
6	15	5	0.015	70% CH_4–15%N_2–15%CO_2
8	20	10	0.020	80% CH_4–5%N_2–15%CO_2
10	25	15	0.025	90% CH_4–5%N_2–5% CO_2
11	30	20	0.030	100%CH_4

5.1 Effects of Pressure on Transient Changes

As an example, the effect of injection pressure variations during gas injection on different parameters was examined. For the verification process described in Section 4, the injection pressure was set to

10 MPa and the injection temperature was set to 20°C. With other parameters kept constant, the wellbore temperature and pressure distributions were simulated for injection pressures of 6, 8, 10, and 11 MPa. The distribution profiles of wellbore temperature, pressure, flow rate and density are shown in Fig. 8.

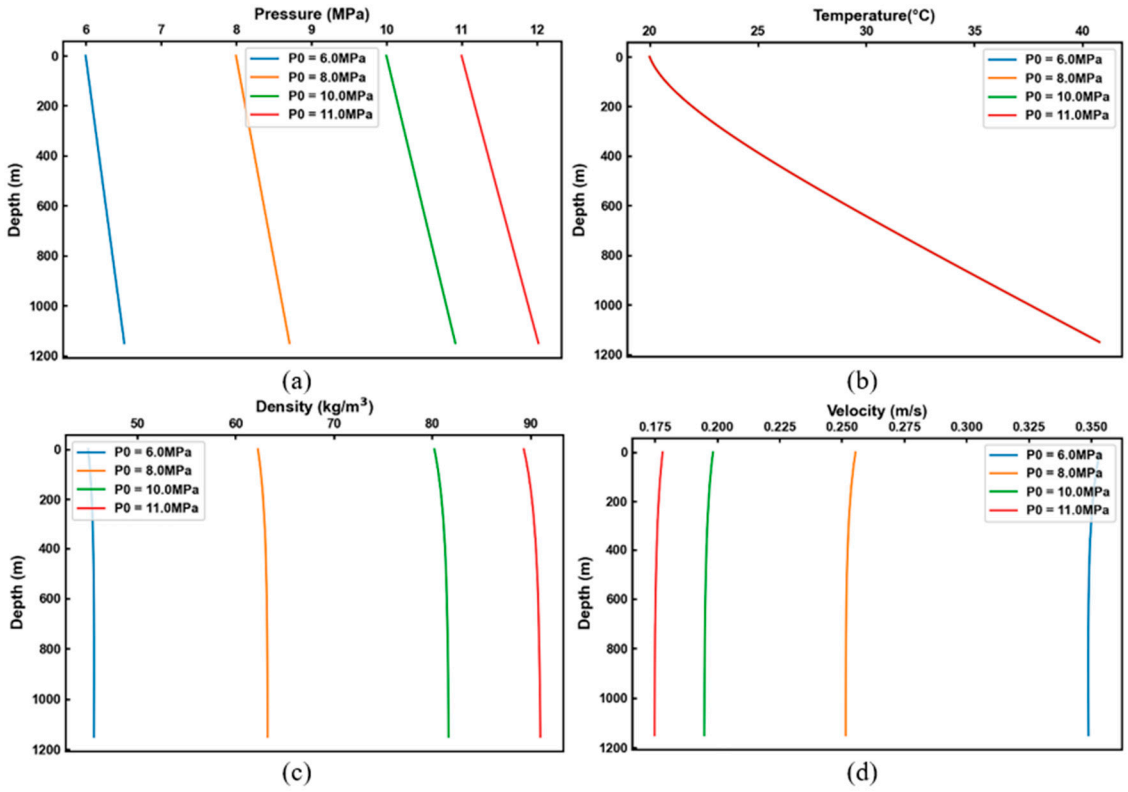

Figure 8: (**a**) Pressure, (**b**) temperature, (**c**) density, and (**d**) velocity distributions along the depth of the wellbore at different injection pressures.

The overall pressure level within wellbore was found to increase synchronously with increasing wellhead injection pressure, with the bottomhole pressure showing a slightly higher rate of increase than that of the wellhead pressure. This occurred because the overall gas density within the wellbore increased with increasing injection pressure, leading to an increase in the hydrostatic pressure gradient along the well depth direction. This resulted in a more pronounced pressure response at the bottom hole.

In contrast, the effect of injection pressure on the temperature field was relatively weak. This is because the wellbore temperature is affected by the heat exchange between the gas and the formation, while pressure variations have a limited impact on heat transfer. The results show that increased pressure only induced minor thermodynamic effects, which resulted in a relatively slight increase in bottomhole temperature. This influence was insufficient to alter the overall pattern of the temperature distribution within the wellbore, rendering changes in the temperature profile negligible.

5.2 Effects of Temperature on Transient Changes

The temperature and pressure distributions within the wellbore were simulated for injection temperatures of 15, 20, 25, and 30°C, keeping all other parameters constant. The distribution profiles of temperature, pressure, flow rate, and density distributions are shown in Fig. 9.

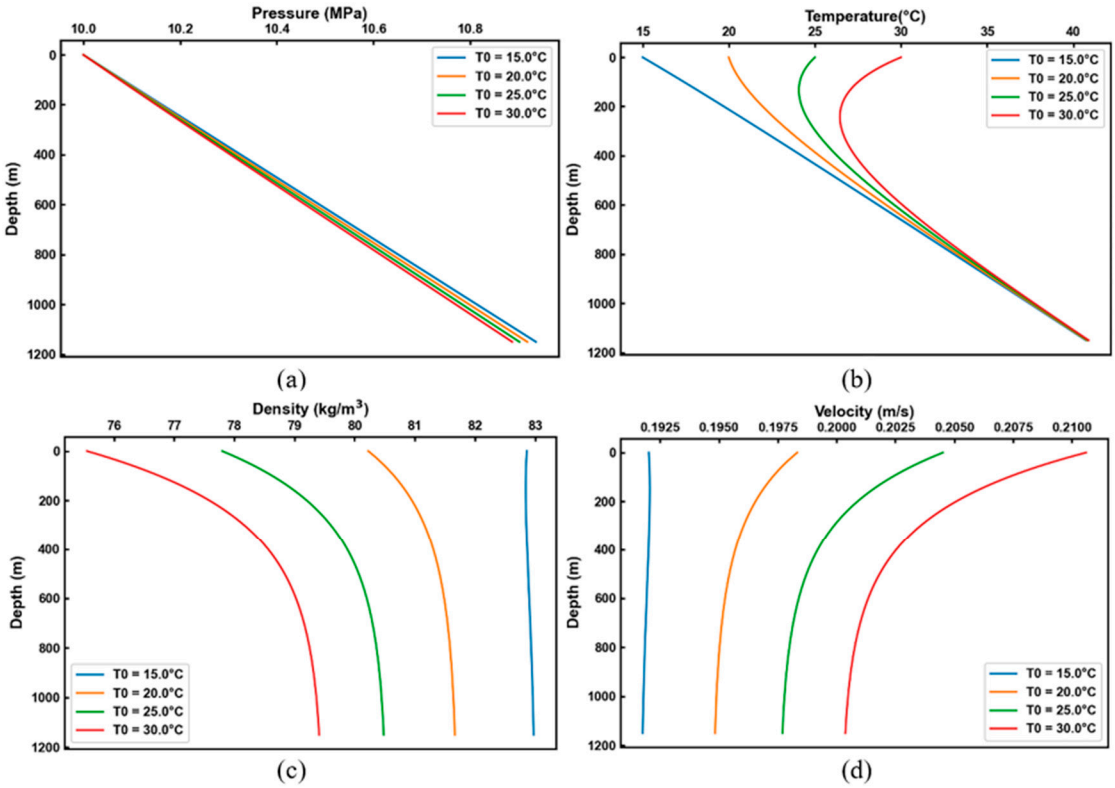

Figure 9: (**a**) Pressure, (**b**) temperature, (**c**) density, and (**d**) velocity distributions along the depth of the wellbore at different injection temperatures.

The increase in injection temperature exerted a systematic effect on the wellbore, which manifested most directly as a noticeable increase in the wellbore fluid temperature near the wellhead. The temperature gradient gradually diminished with depth, leading to a more uniform wellbore fluid temperature near the bottom hole. The increased temperature caused thermal expansion of the gas, which reduced its overall density. This decrease in density reduced the static pressure gradient within the wellbore, which resulted in a slight downward shift in the pressure curve. However, the effect of changes in density was partially offset because the pressure distribution was also affected by frictional pressure loss during fluid flow. Consequently, the overall pressure variation remained relatively small. This indicates that temperature changes primarily affect the gas density by altering the gas properties, rather than directly affecting the wellbore pressure distribution.

5.3 Effects of Injection Quantity on Transient Changes

To investigate the wellbore temperature and pressure distributions during gas injection, simulations were conducted at various flow rates (50,000–250,000 m^3/d) for gas injection, with all other parameters kept constant. The corresponding variations in wellbore temperature, pressure, flow velocity, and density are depicted are as shown in Fig. 10.

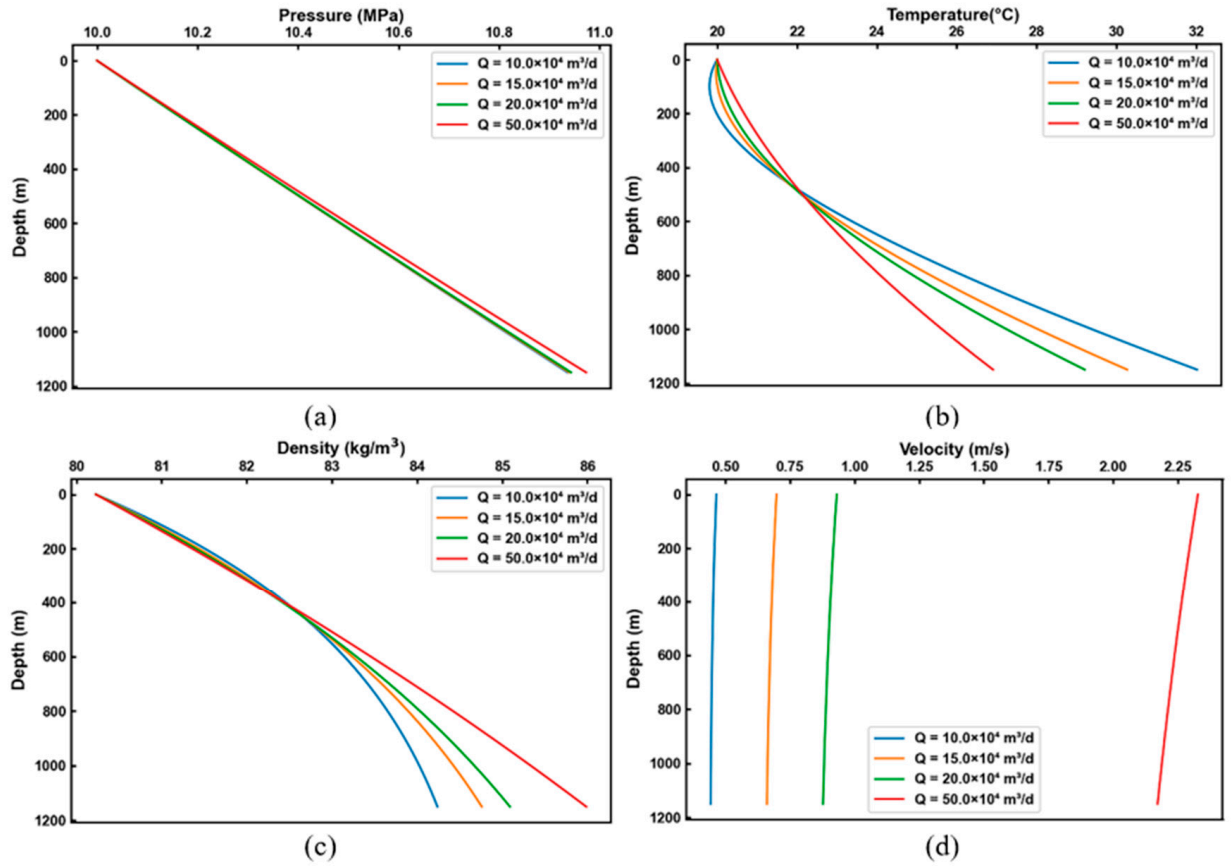

Figure 10: (**a**) Pressure, (**b**) temperature, (**c**) density, and (**d**) velocity distributions along the depth of the wellbore for different gas injection quantities.

The velocity within the wellbore increased significantly as the quantity of gas injected increased, which reduced the residence time of gas in the wellbore. This resulted in insufficient heat exchange between the gas and the formation. Due to an inadequate duration of heat exchange, the gas struggled to fully absorb heat from the formation, which led to an overall decrease in its temperature, as well as a reduced increase in the wellhead temperature.

Meanwhile, the increased flow velocity intensified the effects of frictional flow resistance and altered the pressure drop distribution along the wellbore. Under the influence of reduced temperature, the gas density increased slightly, leading to an upward trend in the bottomhole pressure.

5.4 Effects of Geothermal Gradient on Transient Changes

To investigate the impact of geothermal gradient on transient changes in the wellbore, transient wellbore dynamics were simulated with fixed gas parameters while varying the geothermal gradient to 0.015, 0.020, 0.025, and 0.030°C/m. The resulting distributions of wellbore temperature, pressure, flow velocity, and density are illustrated in Fig. 11.

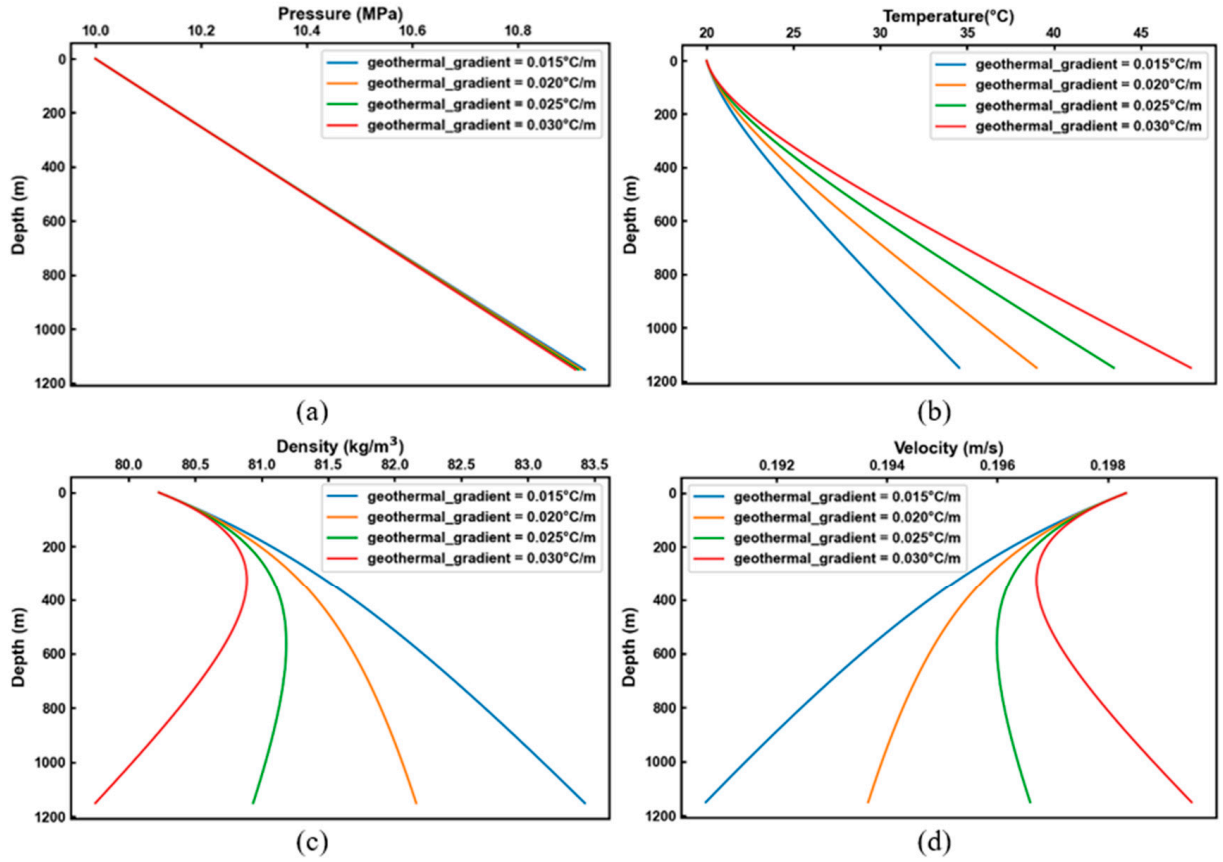

Figure 11: (**a**) Pressure, (**b**) temperature, (**c**) density, and (**d**) velocity distributions along the depth of the wellbore with changes in geothermal gradient.

The geothermal gradient influenced the magnitude of heat exchange between the wellbore and the formation. The temperatures in deeper formations were found to increase with increasing geothermal gradient, which enhanced the heat absorption capacity of the wellbore. This significantly elevated the temperature distribution curve, with the effect becoming increasingly pronounced with greater well depth.

The gas density decreased with increasing temperature, which caused a slight drop in the bottomhole pressure. However, the effect of the geothermal gradient on pressure was far less significant than its effect on temperature. Therefore, the results show that the geothermal gradient was the primary controlling parameter for the temperature field.

5.5 Effects of Injection Components on Transient Changes

To investigate the impact of injected components on transient changes in the wellbore, the transient dynamics were simulated by varying the injected component content while keeping other parameters constant. The corresponding temperature, pressure, flow velocity, and density distributions are shown in Fig. 12.

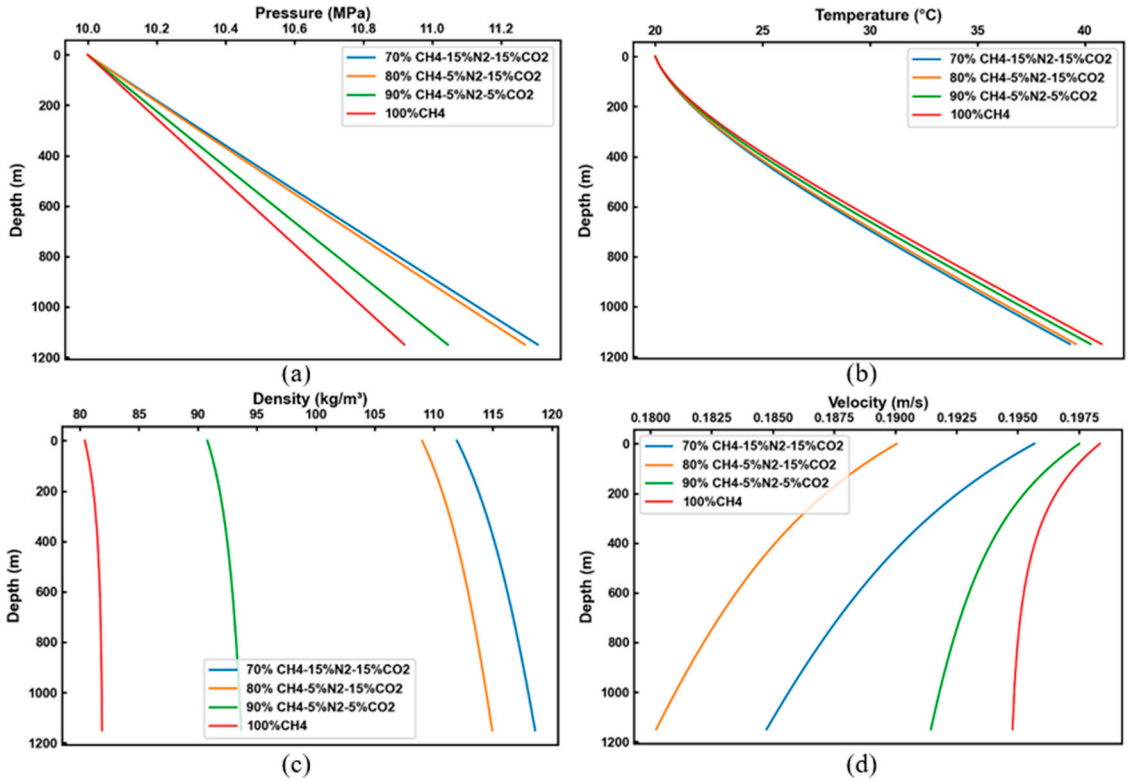

Figure 12: (**a**) Pressure, (**b**) temperature, (**c**) density, and (**d**) velocity distributions along the depth of the wellbore for different injection compositions.

Changes in the injection composition simultaneously affected the thermal properties and state characteristics. As the methane content increased, the gas's average molecular weight decreased, altering its specific heat capacity and compressibility properties. This made the gas more susceptible to heating under identical pressure conditions. Concurrently, compositional shifts also modified the gas density and thereby influenced the static pressure distribution within the wellbore.

As the methane content in the injected gas increased, the overall density of the mixture decreased due to methane's inherently lower density, thereby reducing the wellbore pressure levels. Simultaneously, changes in the injected gas composition altered the gas's specific heat capacity and compressibility characteristics. Meanwhile, variations in the injection composition not only modified the density distribution but also influenced the coupling relationship between temperature and pressure by adjusting the physical parameters of the gas, which resulted in systematic and comprehensive effects on both the wellbore temperature field and pressure field.

5.6 Analysis of Synergistic Effects with Multiple Parameters

To enhance the engineering representativeness of the sensitivity analysis results, two sets of typical parameter combinations were selected to conduct a multi-parameter coupling impact analysis.

5.6.1 Effects of Injection Temperature and Geothermal Gradient

By varying the injection temperature and geothermal gradient, we analyzed the effects of these two factors on the wellbore. The temperature and pressure distributions in the wellbore for temperatures of 15, 25, and 30°C and geothermal gradients of 0.010, 0.020, and 0.030°C/m are shown in Fig. 13.

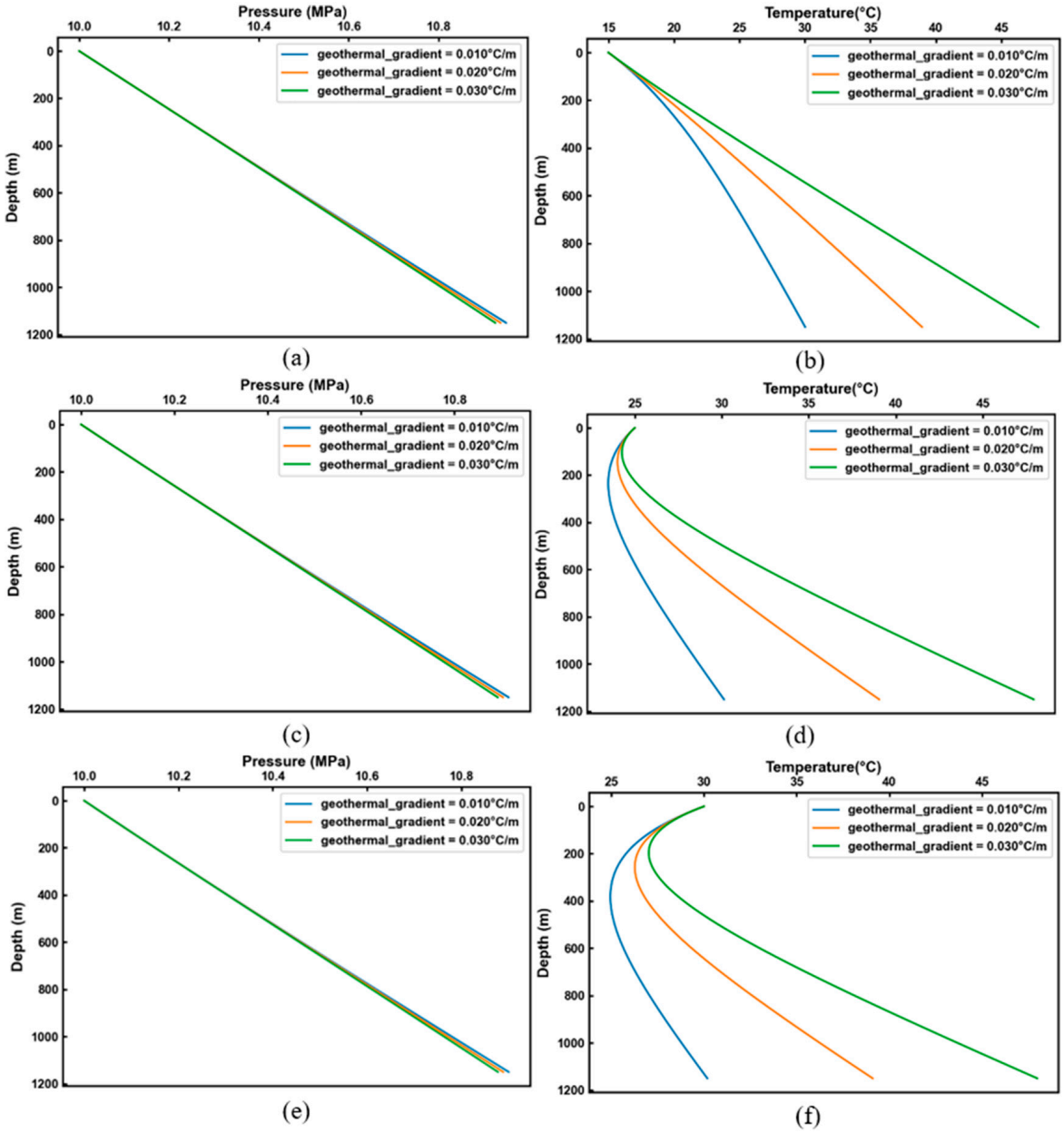

Figure 13: Influence of injection temperature and geothermal gradient on transient changes in the wellbore: (**a**) wellbore pressure distribution at a temperature of 15°C, (**b**) wellbore temperature distribution at a temperature of 15°C, (**c**) wellbore pressure distribution at a temperature of 25°C, (**d**) wellbore temperature distribution at a temperature of 25°C, (**e**) wellbore pressure distribution at a temperature of 30°C, (**f**) wellbore temperature distribution at a temperature of 30°C.

As shown in the Fig. 13, the injection temperature exhibited relatively little effect on the wellbore pressure, with almost no change observed. As the geothermal gradient increased, higher injection temperatures resulted in higher temperatures at the same depth. This difference was most pronounced at shallow depths and then gradually diminished with increasing depth and ultimately converged at greater depths.

5.6.2 Effects of Injection Pressure and Components

The effects of these two factors were analyzed by varying the injection pressure and injection composition. As shown in the Fig. 14, the distribution of temperature and pressure within wellbore was studied for injection pressures of 5, 7, and 9 MPa and for injection compositions of 100% CH_4, 90% CH_4–5% N_2–5% CO_2, and 80% CH_4–5% N_2–15% CO_2.

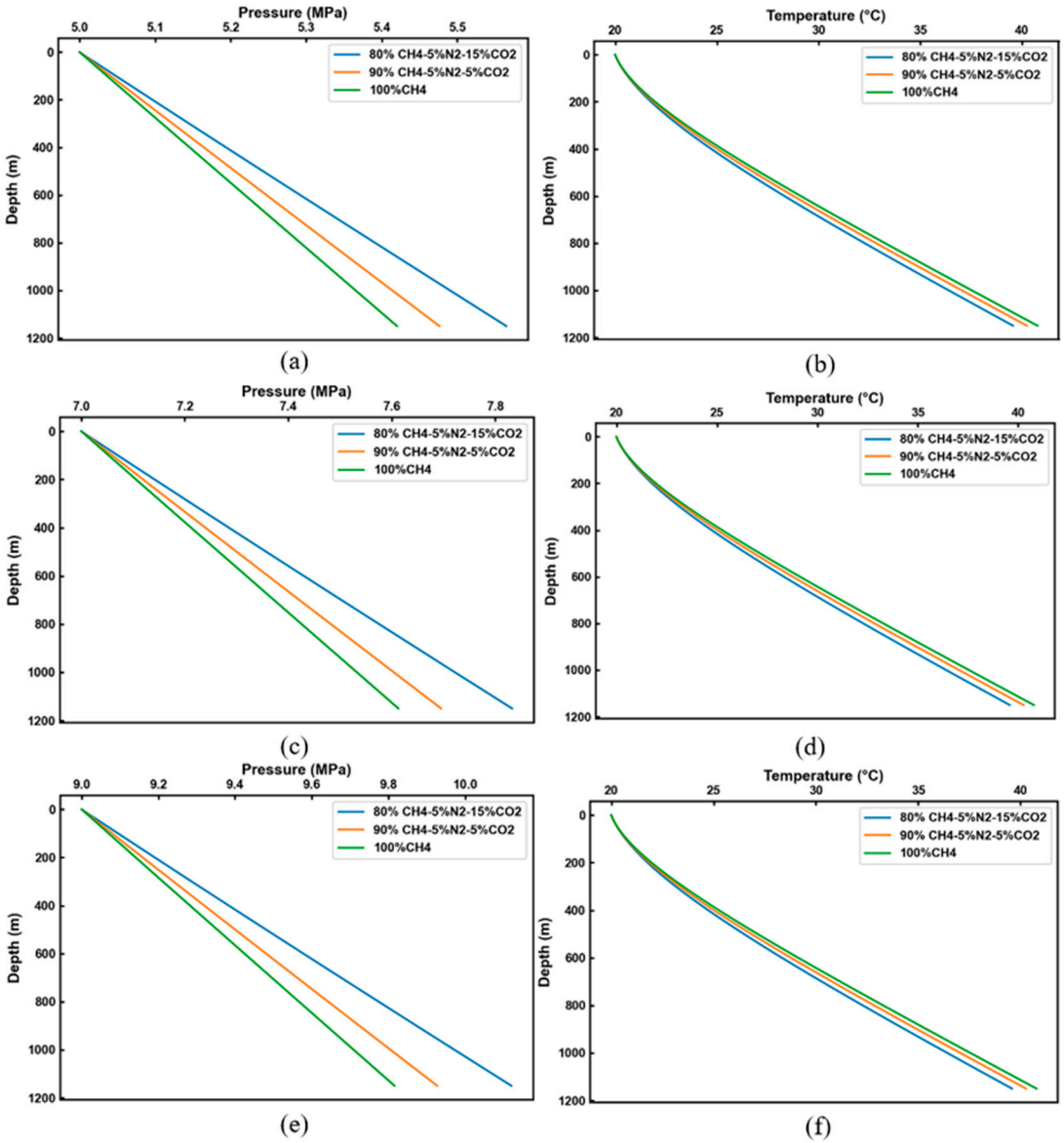

Figure 14: Influence of injection pressure and components on transient changes in the wellbore: (**a**) wellbore pressure distribution at a pressure of 5 MPa, (**b**) temperature distribution in the wellbore at a pressure of 5 MPa, (**c**) wellbore pressure distribution at a pressure of 7 MPa, (**d**) temperature distribution in the wellbore at a pressure of 7 MPa, (**e**) wellbore pressure distribution at a pressure of 9 MPa, (**f**) temperature distribution in the wellbore at a pressure of 9 MPa.

As shown in Fig. 14, changes in the gas composition exerted a certain influence on the pressure distribution but showed no significant effect on the temperature distribution. The injection pressure

increased accordingly with increasing methane content, and the wellbore pressure also increased. However, the bottomhole pressure was lower than that observed with lower methane content.

6 Conclusion

In this study, a wellbore temperature-pressure field prediction model that couples the dynamic thermophysical parameters of multicomponent gas mixtures has been proposed. The model was validated with data from a real facility, and a parametric sensitivity analysis was conducted along with a field application. The main conclusions of this work are summarized as follows:

(1) The proposed model overcomes the conventional simplification of assuming natural gas to be composed purely of methane by fully coupling the dynamic iterative calculation of key thermophysical parameters of multicomponent gases into the equations that govern fluid flow in wellbore environments. The proposed model was validated against measured field data, and the results show that it achieved prediction errors within 3% for both temperature and pressure, significantly outperforming conventional methods.

(2) The sensitivities of key parameters that influence the temperature and pressure fields within a wellbore have been quantitatively clarified. The results show that injection-production flow rate is the most sensitive factor that affects the temperature within a wellbore, while the geothermal gradient dominates the temperature distribution along the depth of the wellbore and injection pressure primarily governs the distribution of the pressure field. Moreover, variations in natural gas components can significantly alter the thermophysical properties of the fluid and exert non-negligible effects on both the wellbore temperature and pressure fields. These results provide a direct theoretical basis for the optimization of gas storage injection-production parameters.

(3) The proposed model and the accompanying software developed in this work have been successfully applied to analyze the injection-production scheme of the X underground gas storage facility and were found to enable accurate simulation of wellbore temperature and pressure profiles. Thus, the results of this work demonstrate that the proposed approach can provide reliable technical information to support safety management for injection-production wells.

Acknowledgement: None.

Funding Statement: The authors received no specific funding.

Author Contributions: The authors confirm contribution to the paper as follows: writing—original draft preparation: Xiang Li; writing—review & editing: Jie Zhang; data curation: Yuxin Cheng, Zhaoqi Xiong; validation: Jiaohao Xie; All authors reviewed and approved the final version of the manuscript.

Availability of Data and Materials: The datasets generated and/or analyzed during the current study are available from the corresponding author on reasonable request.

Ethics Approval: Not applicable.

Conflicts of Interest: The authors declare no conflicts of interest.

References

1. Sedaee B, Almahmoodi Z, Gilavand M, Kanaani M, Mansouri M, Fathi Y. Cushion gas replacement on underground gas storage in a naturally fracture aquifer: cushion gas strategies for matrix-independent storage. Results Eng. 2025;26:105344. [CrossRef].

2. Wang Y, Yang Y, Qin J, Sun Y, Qin G. A probabilistic-based numerical modeling of natural gas pipelines with random corrosion morphology. Int J Press Vessels Pip. 2026;219:105696. [CrossRef].
3. Zamehrian M, Sedaee B. A comparative analysis of gas mixing during the underground hydrogen storage in a conventional and fractured reservoir. Gas Sci Eng. 2024;122:205217. [CrossRef].
4. Kanaani M, Sedaee B. Impact of dilation and irreversible compaction on underground hydrogen storage in depleted hydrocarbon reservoirs. Energy Fuels. 2022;36(22):13506–17. [CrossRef].
5. Ding L, Yang Z, Chen W, Zhang Q. Transient prediction method for flow temperature at wellbore bottom. Appl Therm Eng. 2023;234:121208. [CrossRef].
6. Ramey HJ Jr. Wellbore heat transmission. J Petrol Technol. 1962;14(4):427–35. [CrossRef].
7. Satter A. Heat losses during flow of steam down a wellbore. J Petrol Technol. 1965;17(7):845–51. [CrossRef].
8. Holst PH, Flock DL. Wellbore behaviour during saturated steam injection. J Can Petrol Technol. 1966;5(4):184–93. [CrossRef].
9. Orkiszewski J. Predicting two-phase pressure drops in vertical pipe. J Petrol Technol. 1967;19(6):829–38. [CrossRef].
10. Farouq Ali SM. A comprehensive wellbore steam/water flow model for steam injection and geothermal applications. Soc Petrol Eng J. 1981;21(5):527–34. [CrossRef].
11. O'Reilly D, Haghighi M, Flett M, Sayyafzadeh M. Pressure-transient analysis for cold-water injection into a reservoir coupled with wellbore-transient-temperature effects. SPE Prod Oper. 2021;36(1):197–215. [CrossRef].
12. Sang Y, Du A, Ye C, Xiang J, Chen Y, Guo Y, et al. Temperature and pressure profiles during prolonged working fluid injection in wellbores: mechanisms and key influencing factors. Fluid Dyn Mater Process. 2025;21(7):1623–39. [CrossRef].
13. Al-Adwani F, Langlinais J, Hughes R. Modeling of an underbalanced-drilling operation using supercritical carbon dioxide. SPE Drill Complet. 2009;24(4):599–610. [CrossRef].
14. Span R, Wagner W. A new equation of state for carbon dioxide covering the fluid region from the triple-point temperature to 1100 K at pressures up to 800 MPa. J Phys Chem Ref Data. 1996;25(6):1509–96. [CrossRef].
15. Liu X, Liu L, Yu Z, Zhang L, Zhou L, Zhang Z, et al. Study on the coupling model of wellbore temperature and pressure during the production of high temperature and high pressure gas well. Energy Rep. 2022;8:1249–57. [CrossRef].
16. Zuo W, Dou Y, Liu J, Li L, Zhang W. Research on temperature–pressure coupling model of gas storage well during injection production. Processes. 2024;12(10):2236. [CrossRef].
17. Hong J, Wang Z, Meng L, Shi B, Jing K, Cao C, et al. HTHP coupled fluid-thermal model for predicting wellbore temperature and pressure distribution of underground gas storage. Geoenergy Sci Eng. 2025;253:213999. [CrossRef].
18. Kontogeorgis GM, Folas GK. Thermodynamic models for industrial applications: from classical and advanced mixing rules to association theories. Hoboken, NJ, USA: John Wiley & Sons, Inc.; 2009. [CrossRef].
19. Khosravi A, Machado L, Nunes RO. Estimation of density and compressibility factor of natural gas using artificial intelligence approach. J Petrol Sci Eng. 2018;168:201–16. [CrossRef].
20. Al Ghafri SZS, Jiao F, Hughes TJ, Arami-Niya A, Yang X, Siahvashi A, et al. Natural gas density measurements and the impact of accuracy on process design. Fuel. 2021;304:121395. [CrossRef].
21. Xiong W, Zhang LH, Zhao YL, Hu QY, Tian Y, He X, et al. Prediction of the viscosity of natural gas at high temperature and high pressure using free-volume theory and entropy scaling. Petrol Sci. 2023;20(5):3210–22. [CrossRef].
22. Lee AL, Gonzalez MH, Eakin BE. The viscosity of natural gases. J Petrol Technol. 1966;18(8):997–1000. [CrossRef].
23. Farzaneh-Gord M, Farsiani M, Khosravi A, Arabkoohsar A, Dashti F. A novel method for calculating natural gas density based on Joule Thomson coefficient. J Nat Gas Sci Eng. 2015;26:1018–29. [CrossRef].
24. Li J, Su Y, Yu B, Wang P, Sun D. Influences of hydrogen blending on the joule–Thomson coefficient of natural gas. ACS Omega. 2021;6(26):16722–35. [CrossRef].
25. Wang Y, Ye J, Wu S. A prediction model of wellbore temperature and pressure distribution in hydrocarbon gas injection well. IOP Conf Ser Earth Environ Sci. 2021;766(1):012048. [CrossRef].

26. Hasan AR, Kabir CS. Heat transfer during two-phase flow in wellbores: part I—formation temperature. In: Proceedings of the SPE Annual Technical Conference and Exhibition; 1991 Oct 6–9; Dallas, TX, USA. Richardson, TX, USA: Society of Petroleum Engineers; 1991. p. SPE 22866-MS. [CrossRef].
27. Fourier J. The analytical theory of heat. Cambridge, UK: Cambridge University Press; 1878.
28. Wu L, Luo Z, Zhao L, Yao Z, Jia Y. Study on wellbore temperature & pressure and phase control in supercritical carbon dioxide fracturing. J Southwest Pet Univ. 2023;45(2):117–25. (In Chinese). [CrossRef].
29. Paul K, Pradhan K, Mandal BK. Effect of variation of the aspect ratio of rectangular twisted tapes inserted in a circular pipe on the thermal performance. J Therm Sci Eng Appl. 2025;17(2):021007. [CrossRef].
30. Jain AK. Accurate explicit equation for friction factor. J Hydraul Div Am Soc Civ Eng. 1976;102:674–7. [CrossRef].